VTT Technical Research Centre of Finland

Modal testing and FE-model validation of azimuthing thruster

Nieminen, Vesa; Tervonen, Matti

Published in:
Conference Proceedings of the Society for Experimental Mechanics Series

DOI:
10.1007/978-1-4419-9305-2_1

Published: 01/01/2011

Modal Testing and FE-model Validation of Azimuthing Thruster

Vesa Nieminen, Research Scientist, VTT Technical Research Centre of Finland, Vuorimiehentie 5, Espoo, P.O.Box 1000, FI-02044 VTT, Finland

Matti Tervonen, Principal Lecturer, D. Sc. (Tech.), Seinäjoki University of Applied Sciences, Kampusranta 9A, FI-60320 Seinäjoki, Finland (previously in ABB Marine Oy)

ABSTRACT

Vibratory behavior of an azimuthing thruster was studied with FE-models and the results were verified by full-scale experiments. Studied thruster systems are used both for main propulsion and for steering of vessels. Modeling techniques were developed to take into account the most significant factors and phenomena affecting on the vibration behavior of the structure in real operation conditions. Modeling of structural properties such as bearings, hydraulic steering system, electro-mechanical interaction and rotor dynamics were investigated. The FE-model included also a part of the ship structure. Influence of the surrounding water on the vibration behavior was also studied. A combined FE-model for the structure and surrounding water were constructed and natural frequencies and modes were calculated. Vibration measurements were conducted in dry dock as well as during normal ship operations. Modal parameters in air and in water during operations were determined experimentally. In water the excitation came from ice block impacts and the modal parameters were estimated by Operational Modal Analysis. Operational Deflection Shape analysis was also utilized. Differences between the calculated and experimentally determined modal parameters in air were found to be small. The calculated global natural frequencies in water also corresponded reasonably well with the measured ones.

Introduction

Operating conditions and vessel installations have great effects on the dynamic behavior of marine structures. This is one of the main challenges met when reliable simulation and dimensioning models were developed for Azipod® [1)] azimuthing thrusters, Fig. 1. So, the developed large and complicated FE-models had to be tested and verified in several stages and conditions.

The main goals of this and the larger background study have been:

- to find out all the phenomena that have significant effects on the dynamic behavior of the structure in real operating conditions
- to develop modeling principles and techniques to take into account the phenomena affecting considerably on the vibration behavior of the structure in real operation conditions
- to develop reliable measuring system for use in real severe operating conditions
- to make the simulation models more accurate by developing them according to the measurement results
- to find out explicit numerical values for the effects and significance of the real operating conditions on the dynamic behavior of the system

Full-scale dynamic tests with different analyses, i.e. conventional modal analysis, operating deflections shape analysis (ODS) and operational modal analysis (OMA), were performed both in dry-dock (thruster installed to the vessel but not in the water) and in totally real operation conditions. Modeling techniques and significance of the following topics for the vibration behavior were studied, see also Fig. 1:

- main supporting bearing, i.e. slewing bearing
- hydraulic steering system
- surrounding ship structure
- fluid-structure interaction

1) Azipod® is a registered trademark of ABB

T. Proulx (ed.), *Linking Models and Experiments, Volume 2*, Conference Proceedings of the Society for Experimental Mechanics Series 5,
DOI 10.1007/978-1-4419-9305-2_1,

- rotor bearings
- rotor dynamics
- electro-mechanical interaction between rotor and stator

Studied azimuthing thruster was designed for an ice-breaking vessel. The vessel had two azimuthing thrusters symmetrically both side of the center line of the ship hull. The overall length of the vessel was 100 m. Propulsion power of one thruster was 6.5 MW and mass of the thruster was about 160 tons.

Finite Element Modeling

The whole azimuthing thruster was modeled as well as a part of the surrounding ship structure. Parabolic brick and tetrahedron elements were used for casting parts as well as for forged parts while parabolic shell elements were used for structures made of welded plates. A finite element model of the azimuthing thruster is shown in Fig. 1. The model was created using the commercial finite element software I-DEAS 12 NX. The model contained about 206 000 elements and 445 000 nodes (without model of surrounding water).

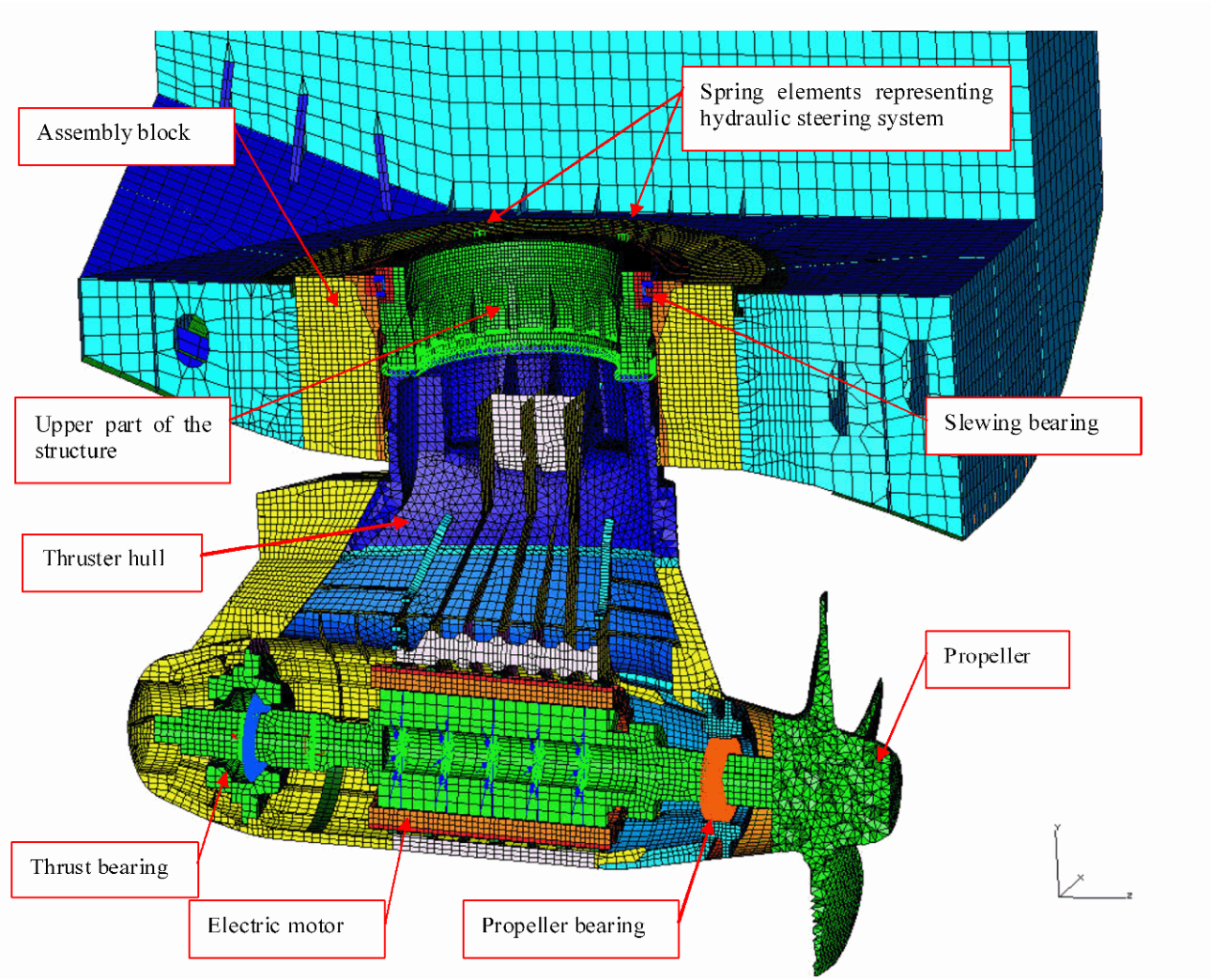

Fig. 1 Finite Element Model of azimuthing thruster and part of the surrounding ship structure (cross section)

Assembly Block and Surrounding Ship Structure

Lowest modes of the azimuthing thruster are strongly affected by stiffness properties of the surrounding structure, i.e. assembly block and the surrounding ship structure. The thruster is supported by the slewing bearing at the upper part of the thruster

structure so that all reaction forces during operation except steering moment goes through the slewing bearing from the thruster to the ship structure.

Modeling of whole ship structure is very laborious work. Therefore only part of the ship structure was modeled around the assembly block, which represents local stiffness properties of the ship structure. Boundary conditions of this section of the ship structure were varied and corresponding results were also compared to the experiments.

Lowest torsional and bending modes of the ship hull could be studied and included to the model for example by using an equivalent beam model. However, global dynamics of the ship hull was excluded from this study.

Slewing Bearing

Slewing bearing consist of three cylindrical rolling bearings, two axial and one radial as shown in Fig. 2. Individual rolling elements were modeled with two spring elements as shown in the figure. Load-deflection relationship of the individual rolling element and for the complete bearing was calculated according to the Herzian contact theory. Contact model between a cylinder and a plane was applied for axial rolling elements [1]. For radial cylindrical rolling elements equations derived in reference [2] was applied. These equations are also based on the Herzian contact theory.

The load-deflection relationships between rolling elements and bearing races are non-linear. The stiffness of individual rolling element contact was linearized around an operation point as follows:

$$k_a(F_a) = \frac{\partial F_a}{\partial \delta_a(F_a)} \tag{1}$$

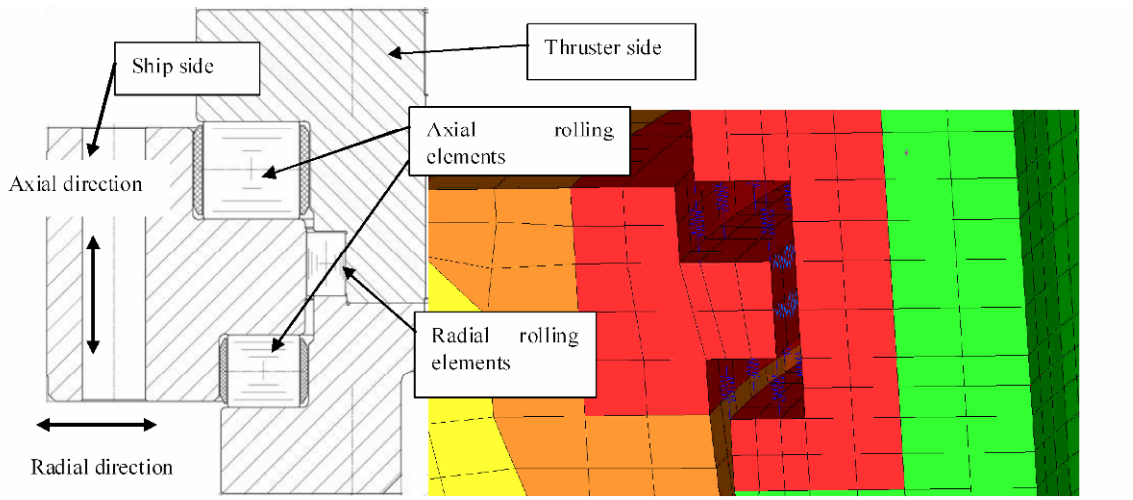

Fig. 2 Slewing bearing

Hydraulic Steering System

Steering moment of the azimuthing thruster is produced by four hydraulic motors. The hydraulic motors are driven by two adjustable-displacement hydraulic pumps, forming a closed hydraulic circuit.

The lowest rotational mode around steering axis is dominated by stiffness of this hydraulic steering system. Most of the flexibility originates from compressibility of the hydraulic fluid, flexibility of the pipelines and hoses. Flexibility of the steering gear mechanism (gear ring and pinions) was assumed to be significantly smaller than flexibility of the hydraulic system and these were neglected in the calculation. The hydraulic fluid "spring" was characterized by the value for the bulk modulus B. Mechanical compliance of the pipelines and hoses were taken into account by calculating radial displacement of the inner surface of the pipe due to internal pressure increase. By using this displacement "bulk modulus" for pipeline B_p and hoses B_h were calculated. The effective bulk modulus for the hydraulic system was then obtained by combining these bulk moduli analogously to the total resistance of parallel resistors as follows [3]:

$$B_e = \frac{1}{\frac{1}{B} + \frac{V_p}{V_{tot}}\frac{1}{B_p} + \frac{V_h}{V_{tot}}\frac{1}{B_h}} \quad (2)$$

where V_p is volume of the pipeline, V_h is volume of the hoses and V_{tot} total volume. By means of specific displacement (displacement/revolution) and specific torque (torque/pressure difference) of the hydraulic motor, stiffness of the hydraulic system was obtained.

Shaft Line

The thrust bearing consist of two spherical roller bearings having contact angle about 45 degrees. Thus, the thrust bearing was capable to carry both axial and radial loads. The propeller bearing was a toroidal roller bearing, so called CARB-type bearing. This type of bearing carries only radial load and allows both axial and angular deflections of the rotor shaft.

Stiffness of the thrust and propeller bearings at operational loads were also determined by the linearization method. The operational loads used for linearization were static reaction forces during normal operation. Cross coupling terms were neglected. Bearings were modeled as spring elements having stiffness coefficients equivalent to the bearing stiffness, radial and axial for thrust bearing and only radial for propeller bearing. One end of this spring element was connected to the shaft and other end by means of constraint equations to the outer race of the bearing housing.

It was found that radial stiffness of the bearings were much higher than bending stiffness of the rotor shaft. Therefore calculation results were not very sensitive to the bearing stiffness values.

Electromechanical Interaction

Magnetic field around the rotor of electrical machine induces electromagnetic forces between rotor and stator. When the rotor is not concentric with the stator bore, the magnetic forces are unbalanced around the rotor. The total force tends to deflect the rotor in the direction of minimum air gap. This force is called unbalanced magnetic pull (UMP). Because the force is directly proportional to the radial displacement of the rotor, it can be modeled by a spring having negative spring constant. Effect of this force is to reduce the effective spring constant of the shaft and thus reduce the rotor natural frequency. The spring constant can be roughly estimated by following equation [5]:

$$k_e = \frac{\pi d_r l_r B_r^{\,2}}{4\mu_0 \delta_0} \quad (3)$$

where d_r is inner diameter of the stator, l_r is stator core length, B_r is amplitude of magnetic flux density, μ_0 is permeability of air and δ_0 is air gap length.

In FE-model the unbalanced magnetic pull was modeled by spring elements between stator and rotor. The elements were distributed in five cross sections and there were 8 spring elements in each cross section equally directed around the cross section so that total negative spring constant in the radial direction equals the estimated value.

In reality the electromagnetically induced force consists of several harmonic components and has components also in axial and tangential directions. However, in this study these components were not taken into account.

Rotordynamics

Influence of gyroscopic forces caused by rotation for vibratory behavior of the shaft line was studied by a separate rotor model. As a consequence of the gyroscopic forces the natural frequencies of the rotor are functions of rotation speed and the natural modes split into forward and backward whirling modes. Considering angular momentum balance of spinning disk, it can be shown that linearized equations of motion for spinning disk become [6]:

$$\begin{Bmatrix} M_x \\ M_y \end{Bmatrix} = \begin{bmatrix} I_d & 0 \\ 0 & I_d \end{bmatrix} \begin{Bmatrix} \ddot{\alpha} \\ \ddot{\beta} \end{Bmatrix} + \Omega \begin{bmatrix} 0 & I_a \\ -I_a & 0 \end{bmatrix} \begin{Bmatrix} \dot{\alpha} \\ \dot{\beta} \end{Bmatrix} \qquad (4)$$

$$M_z = I_a \dot{\Omega}$$

where M_x and M_y are moments around two orthogonal axes perpendicular to the spin axis, α and β are angular deviations around corresponding x and y axes, M_z is moment around spin axis, I_d is diametral moment of inertia, I_a is moment of inertia around spin axis and Ω is angular velocity around spin axis. The second term in the equation (4) representing gyroscopic torques is called gyroscopic matrix. Considering a continuum model, gyroscopic matrix can also be derived for beam element. Equation of motion including the gyroscopic matrix cannot be diagonalized. However, the equation of motion can be written in state space form by defining new state vector $\boldsymbol{q}$ as follows [6]:

$$\begin{bmatrix} \boldsymbol{0} & \boldsymbol{M} \\ \boldsymbol{M} & \boldsymbol{C} \end{bmatrix} \begin{Bmatrix} \ddot{\boldsymbol{u}} \\ \dot{\boldsymbol{u}} \end{Bmatrix} + \begin{bmatrix} -\boldsymbol{M} & \boldsymbol{0} \\ \boldsymbol{0} & \boldsymbol{K} \end{bmatrix} \begin{Bmatrix} \dot{\boldsymbol{u}} \\ \boldsymbol{u} \end{Bmatrix} = \hat{\boldsymbol{A}}\dot{\boldsymbol{q}} + \hat{\boldsymbol{B}}\boldsymbol{q} = 0 \qquad (5)$$

where $\boldsymbol{M}$ and $\boldsymbol{K}$ are mass and stiffness matrices of the system and damping matrix $\boldsymbol{C}$ includes also terms caused by gyroscopic torques according to equation (4). This first order eigenvalue problem can be solved leading to complex eigenvalues and eigenvectors.

The rotor shaft was modeled by beam elements including also gyroscopic matrices. Propeller as well as rotor core was modeled as disk elements. Bearings were modeled as spring elements. Cross coupling terms were neglected. The model did not contain model of thruster body structure nor the ship structure. The model was constructed and solved by using a code created on Matlab environment.

Fluid-Structure Interaction

As the structure which is in contact with fluid vibrates, the fluid surrounding the structure must vibrate as well. This causes increasing of the kinetic energy and degreasing of natural frequencies of the total system. The coupled problem of fluid-structure interaction of thruster and surrounding water was solved by modeling also water domain with finite elements. The fluid was assumed to be compressible and inviscid medium. In addition small displacements were assumed. At an accelerating fluid-structure interface momentum and continuity considerations require that [8]:

$$\frac{\partial p}{\partial n} = -\rho \ddot{u}_n \qquad (6)$$

where p is the dynamic fluid pressure, n is direction of outward normal to the boundary, ρ is fluid density and $\ddot{u}_n$ is the normal component of fluid particle acceleration. At rigid wall right side of equation (6) equals zero. At free surface the surface waves were in this case neglected and the boundary condition used was $p = 0$. Boundary conditions are illustrated in Fig. 3. Generalization of equation (6) to three dimension is given as:

$$\nabla p = -\rho \frac{\partial^2 \{d\}}{\partial t^2} \qquad (7)$$

Definition of bulk modulus in three dimension is $p=-B\nabla\bullet d$. Three-dimensional wave equation can be constructed by taking divergence of equation (7) and differentiating definition of bulk modulus twice with respect to time, leading to:

$$\nabla^2 p = \frac{\rho}{B}\ddot{p} = \frac{1}{c^2}\ddot{p} \qquad (8)$$

where ∇^2 is Laplacian operator and $c = (B/\rho)^{0.5}$ is the wave speed in the fluid. Approximation of the dynamic pressure using the finite element method is then given by [9, 10, 11, 12]:

$$\tilde{p} = \left[\boldsymbol{N}_f\right]\{\boldsymbol{p}\} \tag{9}$$

where matrix $[\boldsymbol{N}_f] = [N_1\, N_2 \ldots N_m]$ includes fluid element shape functions. Substituting approximation (9) into equations (8) and (7), using Galerkin's method of weighted residuals and applying Green's theorem, following equation can be derived:

$$\int_V \left(\{\nabla\}\left[\boldsymbol{N}_f\right]\right)^T \{\nabla\}\left[\boldsymbol{N}_f\right]\{\boldsymbol{p}\}dV - \rho\int_A \left[\boldsymbol{N}_f\right]^T \{\boldsymbol{n}\}^T \left[\boldsymbol{N}_s\right]\{\ddot{\boldsymbol{u}}_s\}dA + \frac{1}{c^2}\int_V \left[\boldsymbol{N}_f\right]^T \left[\boldsymbol{N}_f\right]\{\ddot{\boldsymbol{p}}\}dV = \{0\} \tag{10}$$

where matrix $[\boldsymbol{N}_s]$ includes structure element shape functions and $\{n\}$ denotes a unit normal vector pointing into the structure. Equation (10) can also be written shortly by:

$$\overline{\boldsymbol{Q}}\,\ddot{\boldsymbol{p}} + \overline{\boldsymbol{H}}\,\boldsymbol{p} - \rho\overline{\boldsymbol{L}}\,\ddot{\boldsymbol{u}}_s = \{0\} \tag{11}$$

In the structure point of view, a nodal force vector equivalent to the fluid pressure can be expressed using the pressure approximation (9) as:

$$\{\boldsymbol{r}_t\} = \int_A \left[\boldsymbol{N}_s\right]^T \{\boldsymbol{n}\}\boldsymbol{p}dA = \int_A \left[\boldsymbol{N}_s\right]^T \{\boldsymbol{n}\}\left[\boldsymbol{N}_f\right]dA\{\boldsymbol{p}\} = \overline{\boldsymbol{L}}^T\{\boldsymbol{p}\} \tag{12}$$

If external force of the structure and damping will be neglected, so called pressure formulation for the coupled fluid-structure problem can be expressed as [9]:

$$\begin{bmatrix} \boldsymbol{M} & \boldsymbol{0} \\ -\rho\overline{\boldsymbol{L}} & \overline{\boldsymbol{Q}} \end{bmatrix}\begin{Bmatrix} \ddot{\boldsymbol{u}} \\ \ddot{\boldsymbol{p}} \end{Bmatrix} + \begin{bmatrix} \boldsymbol{K} & \overline{\boldsymbol{L}}^T \\ \boldsymbol{0} & \overline{\boldsymbol{H}} \end{bmatrix}\begin{Bmatrix} \boldsymbol{u} \\ \boldsymbol{p} \end{Bmatrix} = \{0\} \tag{13}$$

where $\boldsymbol{M}$ and $\boldsymbol{K}$ are structural mass and stiffness matrices. Equation (13) is unsymmetric and therefore it is difficult to solve. However, the fluid-structure matrix system can be symmetrized for instance by defining new fluid unknown as presented in reference [13].

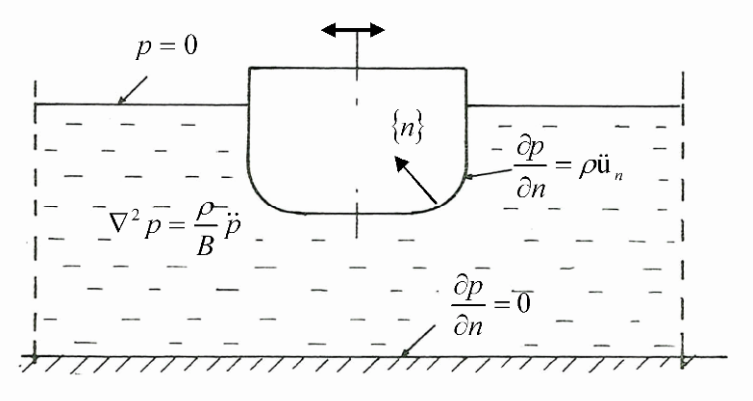

Fig. 3 Boundary conditions of the fluid

ABAQUS software was used to create and solve FE-model of combined structure and fluid [14]. Fluid was modeled with acoustic tetrahedron elements. Modeling of the water was first studied by a simple structure such as sphere and circular disk. Meshing properties such as element size, size of the water model and element order as well as boundary conditions at exterior surfaces of the water model were varied. Results of these simple finite element studies were compared with analytical solutions and with some experimental results found in the literature [7, 15, 16, 17, 18]. It was found that if the model of the fluid is large enough, boundary conditions at outer surfaces of the fluid has not significant effect on the natural frequencies of the structure. On the basis of these studies, water model for the azimuthing thruster was constructed. The water model contained about 267 000 elements and 55 000 nodes.

Experimental Studies

Experimental Modal Analysis in Dry Dock

Modal testing of the azimuthing thruster was carried out in dry dock. The thruster was excited by a pendulum made by mass of 50 kg, see Fig. 4. The steering mechanism was locked during testing. Excitation force was measured by an accelerometer installed on the end of the mass and response of the azimuthing thruster was measured by 10 triaxial accelerometers. Sampling frequency used was 512 Hz. Signal processing and FRF calculation was carried out by using LMS Scadas III front-end and LMS Cada-X software. Modal parameters (frequencies, modal damping ratios and mode shapes) were estimated using LMS TestLab and LMS Cada-X softwares [19, 20]. The parameters were estimated by using PolyMAX algorithm [21].

Frequency range of interest was from zero to the most significant excitation frequencies during normal operation. One of the most significant excitation was blade frequency.

Identified modes are presented in Table 1. For reasons of confidentiality all frequencies and modal damping factors in this paper are presented as scaled values. The reference frequency f_{ref} used in scaling is the natural frequency of first longitudinal mode of the azimuthing thruster measured in dry dock. Also the reference modal damping factor ζ_{ref} is the damping factor of first longitudinal mode of the azimuthing thruster measured in dry dock. Lowest transversal mode shape is shown in Fig. 6.

In order to quantify orthogonality or independency of measured modes, AutoMAC criterion [22, 23] was applied, see Fig. 5. MAC takes values between 0 and 1; the closer to 1 means high correlation, while the closer to 0 means that those modes are orthogonal or independent. As can be seen, between modes 1 and 2 there is quite high MAC value. These modes are global mode of the ship hull and lowest transversal mode of the thruster. Also there is quite high off-diagonal term in AutoMAC matrix between modes 6 and 7. These modes relates to vertical bending modes of the rotor. High off-diagonal values originate from the fact that the number of measuring points is too small to identify these modes (spatial aliasing). In order to identify global modes of the ship there should be more measuring points on the ship hull. Also there should be more measuring points on the rotor and propeller blades in order to identify more accurately rotor bending modes. However, used measuring points was noticed to be sufficient for identifying satisfactory the lowest modes.

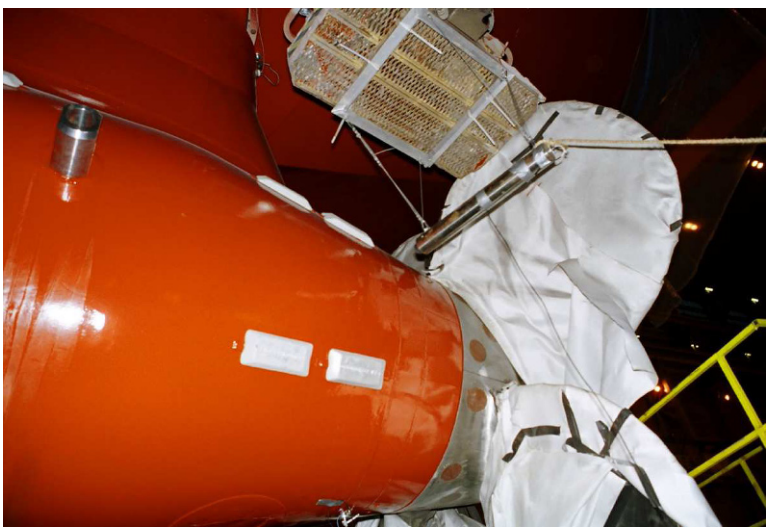

Fig. 4 Impact testing of thruster by using pendulum

Table 1 Measured modes of azimuthing thruster in air

Mode no	Frequency (f_i/f_{ref})	Modal damping (ζ_i/ζ_{ref})	Description
1	0,636	0,1	Global mode of astern ship hull
2	0,826	0,3	1st transversal mode
3	0,906	1,7	Rotation around steering axis
4	1,000	1,0	1st longitudinal mode
5	1,182	1,1	Global mode of the ship hull
6	2,217	1,5	Vertical bending of the rotor, vertical translation of the thruster in phase
7	2,501	0,8	Vertical bending of the rotor, vertical translation of the thruster out of phase
8	3,061	1,4	Transversal bending of the rotor, rotation of the thruster around steering axis out of phase
9	4,643	1,1	First elastic mode of the thruster hull, torsion around vertical axis

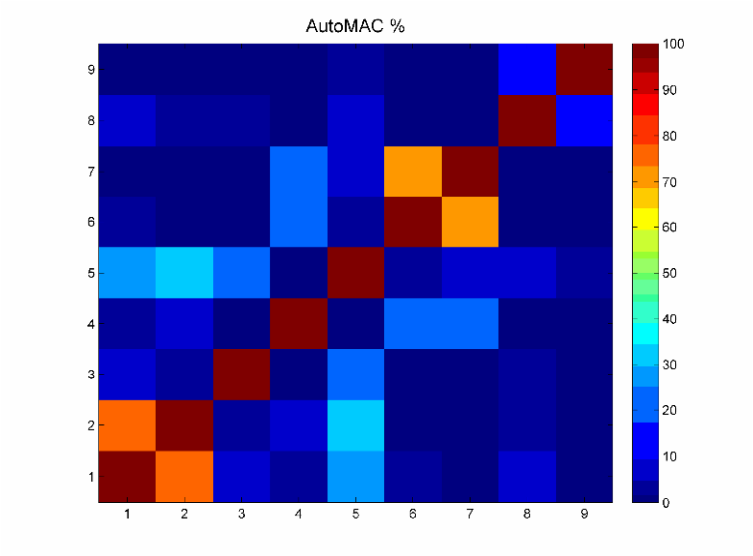

Fig. 5 AutoMAC for measured mode shapes

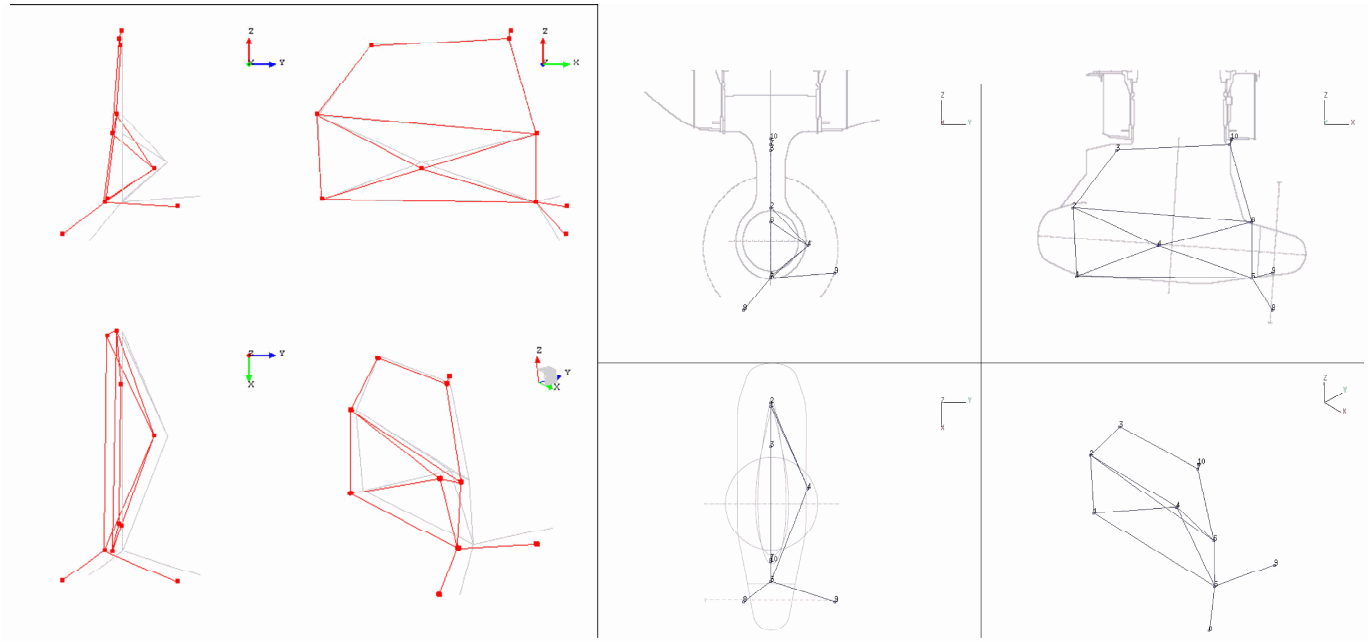

Fig. 6 Lowest transversal mode in air (left). Measuring points 8 and 9 are on two propeller blades. Point 10 is on the bottom of the ship hull

Calibration measurements by static forces

The azimuthing thruster was instrumented by several strain gages and other measuring devices for long-term ice load monitoring. The ice load measuring system was calibrated by applying external static forces on the propulsion unit in dry dock. The applied forces were measured by load cells. Radial relative displacement between the thruster body and the ship hull was also measured during calibrations with two inductive displacement sensors, see figure Fig. 7. These measurements provided information about flexibility of slewing bearing as well as thruster body for verification of the used FE-model.

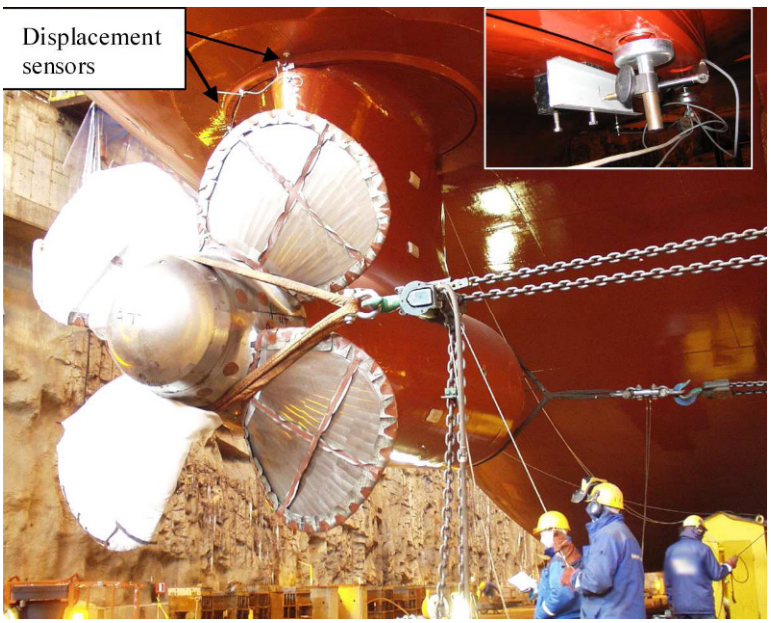

Fig. 7 Calibration of ice load measuring system in transversal direction

Measurements During Ship Operation

Vibrations of azimuthing thruster were measured during normal operation by accelerometers. Accelerations of propeller bearing housing as well as thrust bearing housing were measured by triaxial accelerometers. Vibrations of slewing bearing near the outer race were measured at four locations by uniaxial accelerometers. Shaft displacements relative to the bearing housings were measured by eddy current displacement sensors. Radial displacements at propeller bearing and thrust bearing were measured in two perpendicular directions. In addition axial displacement was measured at propeller bearing. Hydraulic pressure of the steering system was also measured. Several most important operational parameters of azimuthing thrusters and ship were also recorded, for example rotation speeds of the propellers and azimuthing angles.

During normal operation in ice conditions the most significant excitation came from the ice block impacts. When the propeller penetrated in the ice, the rotation speed of the propeller varied widely due to ice loads. Therefore the blade frequency and other harmonic excitation frequencies also changed, exciting the natural modes of the thruster. In this driving condition the excitation resembled periodic chirp excitation signal [23].

A typical 28 min long period where the vessel proceeded in ice was selected for the vibration analysis. Spectral map (vibration spectra as a function of time) for transversal acceleration of the propeller bearing is presented in Fig. 8. Fluctuation of the blade frequency component can be detected in the figure. The rotation speed varied between about 0.5…1 times the nominal speed. The first transversal mode of the azimuthing thruster at about 0.7 f_i/f_{ref} can be can be seen in the map.

Averaged autospectra are presented in Fig. 9. The number of averages was about 1700. On the averaging process the rotational speed related vibration components were averaged out due to relative high fluctuation of rotation speed. Most of the significant peaks in the averaged autospectra are natural frequencies of the thruster.

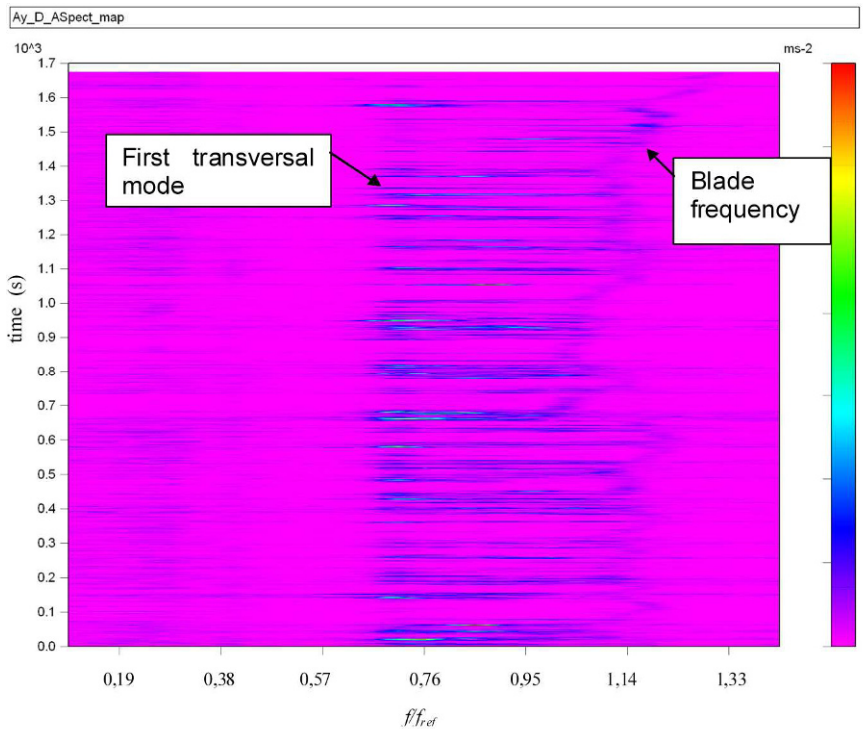

Fig. 8 Spectral map of transversal acceleration of propeller bearing.

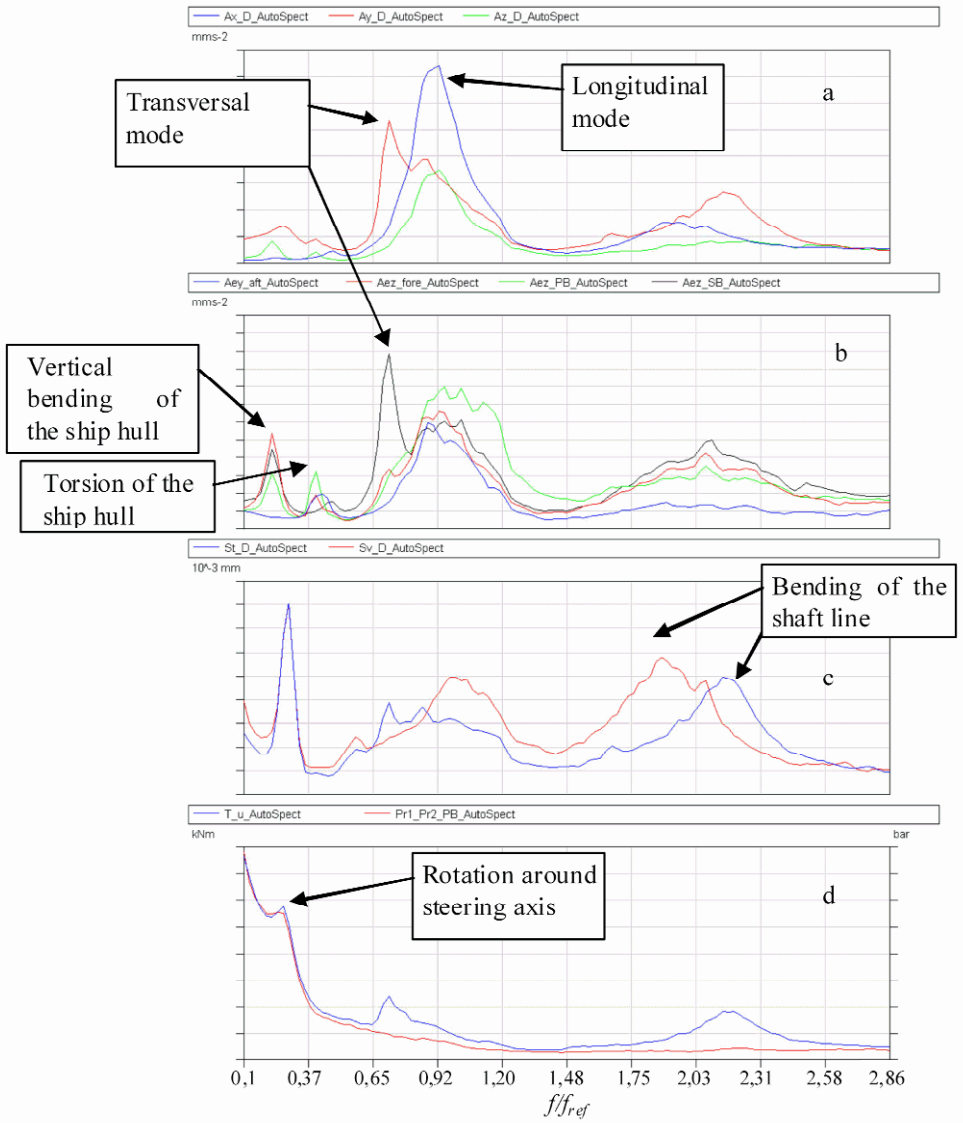

Fig. 9 Averaged autospectra. a: propeller accelerations (Ax = axial, Ay = transversal, Az = vertical), b: slewing bearing accelerations, c: relative shaft displacements at propeller bearing (St = transversal, Sv = vertical), d: torque of the thruster body around steering axis (T_u) and hydraulic pressure of the steering system (Pr1_Pr2)

Operating Deflection Shapes (ODS) at frequencies of most significant peaks in the averaged spectra were determined. It was found that these modes resembled natural mode shapes of the thruster.

Operational Modal Analysis (OMA) was also carried out in order to identify natural modes of the thruster during operation. Measured accelerations of 6 points were used and PolyMAX algorithm was applied for modal parameter identification [24]. Identified modal parameters are given in Table 2. Natural modes in air obtained from modal testing in dry dock are also presented in the table for comparison.

Lowest rotor bending modes were estimated by separate analysis. Before this analysis all measured accelerations were integrated twice and relative shaft displacement signals were summed to absolute bearing displacements in order to get absolute shaft displacements. Modal parameters of rotor bending modes were then estimated by PolyMAX algorithm by using these signals. It should be noted that the used OMA method does not include assumptions of nonlinearities and whirling modes. Therefore, obtained modal parameters of rotor bending modes contain uncertainties. However, it is possible that the natural frequencies obtained may be reasonably reliable.

Due to practical limitations the number of measuring points during operation was rather small. In order to get more accurate mode shape and damping estimates especially for higher modes it is recommended that more measuring points should be included in the analysis. However, in this case the used configuration was able to identify parameters for lowest modes of the thruster reasonably well, especially natural frequencies.

Table 2 Experimental modal analysis results

In dry dock		During operation in water (OMA)		
frequency (f_i/f_{ref})	damping (ζ_i/ζ_{ref})	frequency (f_i/f_{ref})	damping (ζ_i/ζ_{ref})	description
-	-	0,218	0,97	Global mode of the ship hull (apparently vertical bending)
0,906	1,69	0,279	4,31	Rotation around steering axis
-	-	0,402	0,34	Global mode of the ship hull (apparently torsion)
0,826	0,34	0,707	0,71	1st transversal mode
1,000	1,00	0,911	1,63	1st longitudinal mode
2,217	1,51	1,944	1,49	Vertical bending of the rotor, vertical translation of the thruster in phase
2,501	0,83	-	-	Vertical bending of the rotor, vertical translation of the thruster out of phase
3,061	1,40	2,178	1,40	Transversal bending of the rotor, rotation of the thruster around steering axis out of phase

Numerical Results and Correlation with Experiments

Azimuthing Thruster in Air

Before analyses the mass of the model of the mechanical structure was calculated. It was noted that the mass of the model was about 2 % smaller than weighted mass of the real structure. Considering the simplifications in the model the difference is quite small.

The ship had two azimuthing thrusters symmetrically both side of the centre line of the ship hull. Symmetrical boundary condition was applied at the centre line of the ship structure model in most of the analyses. Symmetric boundary condition implies that the thrusters vibrate transversally out of phase. At the other edges of the ship model displacements were fixed. Natural modes were also calculated with anti-symmetric boundary condition at the centre line, which implies that the thrusters vibrate in phase. The calculated transversal mode of the thruster with anti-symmetric boundary condition was about 2% higher than with symmetric boundary condition. Differences for the other global modes were negligible. Thus, it was concluded that coupling between the thrusters modes was rather small.

Influence of stiffness of the slewing bearing on the thruster modes was studied. Because the stiffness of the bearing depends on the loading, the stiffness was calculated with different loading scenarios. At first, gravity of the thruster was applied as evenly distributed load for the upper axial bearing. The lower axial bearing was assumed to have a clearance between rolling elements and bearing races, thus having no contact force and no stiffness. The goal was to simulate the corresponding modal testing condition in dry dock. It was found that frequency of the lowest transversal mode was about 6 % higher than the measured one and frequency of the longitudinal mode was about 3 % smaller than the measured one. Calibration measurements with static external force were also simulated in order to study static stiffness of the thruster. Results showed that the static stiffness in the transversal direction was about 9 % higher than measured one and stiffness in the longitudinal direction was about 4 % smaller than measured one.

Sensitivity analysis showed that stiffness of the axial slewing bearing had significant effect on the natural frequencies, while stiffness of the radial slewing bearing had only minor effect. It was noted that displacements between the upper rolling elements and the bearing race due to gravity of the thruster were very small, significantly smaller than for instance flatness tolerance of the raceway. Also due to challenging construction and installation of the assembly block and the slewing bearing, it is very difficult to determine the real stiffness distribution of the slewing bearing. However, it is possible to study possible variation range of the stiffness. Assuming that gravity of the thruster is evenly distributed for rolling elements of the upper axial bearing and lower axial rolling elements to be just in contact with very low contact force, the stiffness of the whole slewing bearing was found to increase about 52 % compared to the previous case. Assuming that rolling elements of upper axial bearing are just in contact with very low contact force and lower axial bearing having a clearance between rolling elements and raceway, the stiffness was found to degrease about 45 %. By changing the stiffness of individual rolling elements of axial slewing bearing in the model within limits described above, close results with experiments were achieved, see Table 3. Difference between calculated and simulated static stiffness of the thruster was also smaller, about 4.7 % in the transversal direction and 0.5 % in the longitudinal direction.

MAC-criterion was used to evaluate the correlation between experimentally determined and calculated mode shapes, see Fig. 10. As can be seen, diagonal values are over 70 % indicating good correlation for all modes except mode no 6 (transversal bending of the rotor). The rotation angle of the propeller was slightly different during testing compared to the model, which can be one possible reason for the low MAC value. Experimentally determined mode shapes were complex whereas numerically obtained were real modes. This can also contribute the MAC values.

Table 3 Numerical and experimental natural frequencies in air

No	Description	Numerical Frequency (f_i/f_{ref})	Experimental Frequency (f_i/f_{ref})	Difference (%)
1	1st transversal mode	0,840	0,826	1,7
2	Rotation around steering axis	0,929	0,906	2,6
3	1st longitudinal mode	0,990	1,000	-1,0
4	Vertical bending of the rotor, vertical translation of the thruster in phase	2,158	2,217	-2,7
5	Vertical bending of the rotor, vertical translation of the thruster out of phase	2,571	2,501	2,8
6	Transversal bending of the rotor, rotation of the thruster around steering axis out of phase	2,935	3,061	-4,1

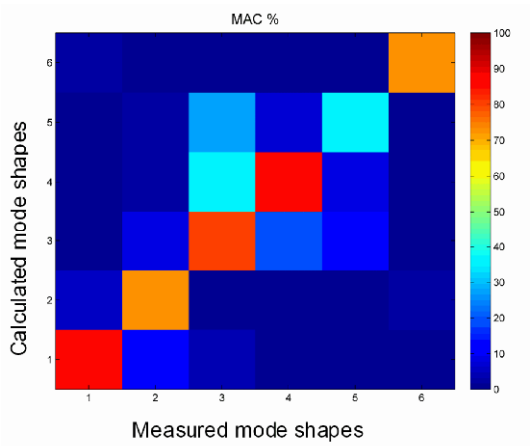

Fig. 10 MAC values between experimental and numerical mode shapes in air

Both experimental and numerical results showed that rotor modes are strongly coupled with the thruster. Therefore there is significant difference between frequencies of rotor transversal and vertical bending modes. In addition, the first vertical

bending mode was split into two modes, in the other mode the thruster body translates in phase and in the other mode the thruster body translates out of phase. Significant errors will be encountered if natural modes of the shaft line will be calculated without taking into account the whole azimuthing thruster and ship structure. Effect of the thruster body and surrounding structure on rotor bending modes are presented in Table 4.

Table 4 Effect of the thruster body and surrounding structure on rotor bending modes

Rotor model only, supported by bearings (spring elements)		Whole model of the azimuthing thruster (rotor + thruster body + part of the ship structure)		Measured, in air
freq. (f_i/f_{ref})	description	freq. (f_i/f_{ref})	description	freq. (f_i/f_{ref})
2,296	1st vertical bending	2,158	1st vertical bending, vertical translational mode of the thruster body in phase	2,217
		2,571	1st vertical bending, vertical translational mode of the thruster body out of phase	2,501
2,305	1st transversal bending	2,935	1st transversal bending, rotation of the thruster around steering axis out of phase	3,061
4,695	2nd vertical bending	4,856	2nd vertical bending	
4,776	2nd transversal bending	5,224	2nd transversal bending	

Results of separate rotordynamic studies are presented in Fig. 11. The Campbell diagram presents lowest natural frequencies of the rotor as a function of the rotation speed. Excitation frequencies of rotation speed as well as blade frequency are also shown in the diagram. Intersection of these lines and curves of natural frequencies indicates critical speeds. As can be seen, the natural modes were split into forward and backward whirling modes. Difference between forward and backward whirling frequencies of first mode at typical rotation speed was about 7 %. These results were not verified by experiments, but influence of the gyroscopic forces on natural frequencies can be evaluated by presented studies.

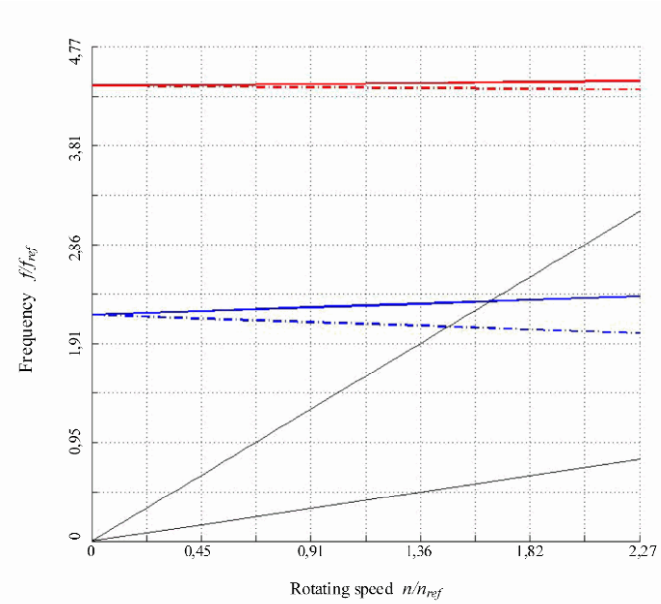

Fig. 11 Campbell diagram. Reference rotation speed n_{ref} is maximum rotation speed

Natural frequencies of the shaft line were calculated with and without UMP. Due to UMP the natural frequencies of shaft line was degreased only about 0.4 %. The banding stiffness of the rotor in this case was very high compared to the forces of UMP. Therefore, electromechanical interaction has only minor effect on the natural frequencies for this type of azimuthing thrusters.

A response analysis was carried out by using modal superposition method. Modal damping factors determined through experimental modal analysis were used. Excitation and response points were the same which were used modal testing in dry dock. Fig. 12 shows the Frequency Response Function (FRF) comparison at point near the propeller bearing. Excitation force has been directed in the transversal direction and acceleration response has also measured and calculated in the transversal direction. The lowest peaks in the measured FRF indicate global natural modes of the ship hull. These peaks can not be seen in the calculated FRF, because the model contained only small part of the ship structure.

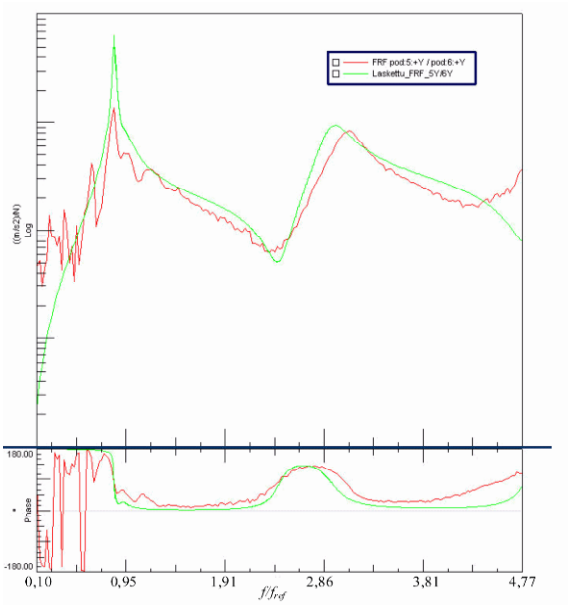

Fig. 12 FRF comparison of measured (red line) and FE-analysis (green line)

Azimuthing Thruster in Operation in Water

Comparison of calculated and experimentally determined natural modes during operation in water is presented in Table 5. The 6th column presents differences between natural frequencies in air and in water calculated by FE-model. The corresponding differences for experimentally determined natural frequencies are shown in the last column. As can be seen, the calculated natural frequencies of lowest global modes in water corresponded reasonably well with the measured ones. Due to added mass of the surrounding water, natural frequencies of the lowest longitudinal and transversal modes were degreased in this case about 5 % and 14 %, respectively. The lowest rotational mode around steering axis is dominated during operation by stiffness of the hydraulic steering system. During modal testing in dry dock the steering mechanism was locked. Therefore the natural frequency of this mode in water is significantly smaller than in air.

Calculated frequency of the lowest vertical bending of the rotor was about 6 % lower than experimentally determined one. Difference for transversal bending mode was even higher. Influence of the gyroscopic forces was not taken into account in this calculation. This can be one possible reason for the differences. It is possible that influence of the gyroscopic forces for the coupled shaft line bending and thruster translational modes is different than the previously presented studies with the shaft line model indicated.

Because vertical bending modes of the shaft line are coupled with vertical translation of the thruster, there are also significant deformations of the ship bottom. Therefore it is important that the structural-acoustic coupling is used between ship bottom and water model. Natural modes were also calculated without the coupling between ship bottom and water. It was found that the frequency of the vertical bending mode of the shaft line was increased as much as 14 % compared to the analysis where the coupling between the ship hull bottom and water was taken into account.

Table 5 Natural modes during operation in water

No	Description	FE-model, **in water** frequency (f_i/f_{ref})	Experi-mental **in water** frequency (f_i/f_{ref})	Difference FE-model - Experimen-tal **in water** (FE – Exp) (%)	**FE-model** Diff. in air – in water (in water – in air) (%)	**Experimental** Diff. in air – in water (in water – in air) (%)
1	Rotation around steering axis	0,277	0,279	-0,9	-69,7	-69,2
2	1st Transversal mode	0,724	0,707	2,4	-13,5	-14,3
3	1st Longitudinal mode	0,940	0,953	-1,4	-4,6	-4,7
4	Vertical bending of the rotor, vertical translation of the thruster in phase	1,806	1,920	-5,9	-17,1	-13,4
5	Vertical bending of the rotor, vertical translation of the thruster out of phase	2,098	-	-	-16,9	-
6	Transversal bending of the rotor, rotation of the thruster around steering axis out of phase	2,498	2,186	14,3	-15,3	-28,6

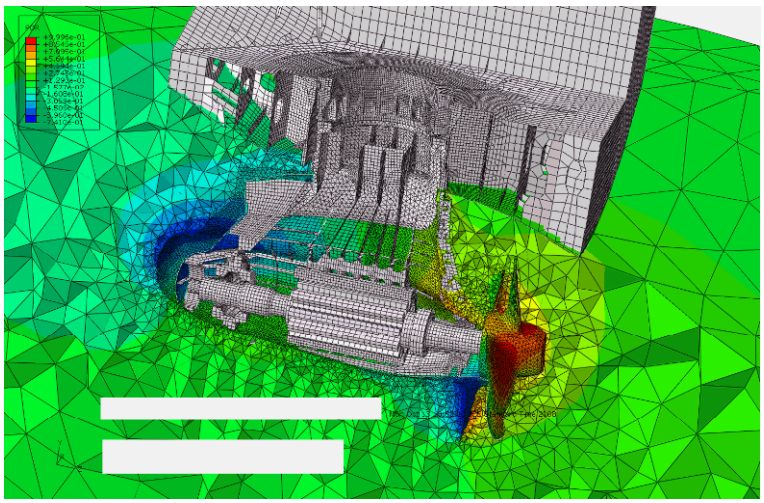

Fig. 13 First longitudinal mode shape in water. Pressure in the acoustic medium is presented as colors

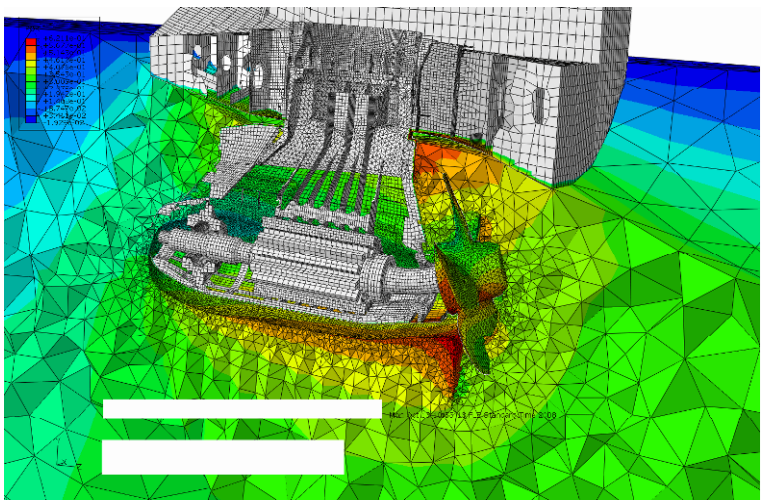

Fig. 14 Vertical bending mode of the rotor coupled with vertical translation of the thruster in phase

Conclusions

Close results were obtained from finite element analyses and experimental investigations. Maximum difference between calculated and experimentally determined natural frequencies in air was about 4 %. The calculated global natural frequencies in water also corresponded reasonably well with the measured ones. Due to the surrounding water natural frequencies of the lowest longitudinal and transversal modes were degreased in this case about 5 % and 14 %, respectively. Based on the modeling method presented in this paper, sufficiently accurate calculation results can be achieved.

From the modeling point of view the following conclusions can be made:

- Slewing bearing stiffness and local stiffness of ship affect significantly natural frequencies and modes
- Shaft line bending modes are strongly coupled with the global modes of the thruster body
- Fluid-structure interaction can be modeled with sufficient accuracy with the used modeling method
- Stiffness of the hydraulic steering system dominates the thruster rotation modes around steering axis
- Electromechanical interaction has only minor effect on the natural frequencies for this type of azimuthing thrusters

The presented case study proved applicability of OMA and ODS analyses in challenging operating conditions where conventional modal testing is practically impossible. These analyses provided necessary information for model verification. Due to practical limitations, the number of measuring points during operation was rather small. In order to get more accurate mode shape and damping estimates especially for higher modes, it is recommended that more measuring points should be included in the analysis. However, in this case used configuration was able to identify parameters for lowest modes of the thruster reasonably well.

In the future studies it is recommended that the gyroscopic effect will be taken into account with the whole model of the azimuthing thruster. This can be done for example by combining rotor model and the thruster body model using substructuring technique.

Acknowledgements

This paper is based on Master's Thesis "Modelling of Vibratory Behaviour of Azimuthing Thruster", in finnish. The thesis has been done for Helsinki University of Technology for department of Applied Mechanics in 2009. Financial support for this study was provided by ABB Marine.

References

1. Pilkey, Walter D. Formulas for stress, strain and structural matrices. John Wiley & Sons Inc, New York, ISBN 0-471-52746-7 1458 p. 1994.

2. Harris, Tedric A. Rolling Bearing Analysis. 4th Edition. John Wiley & Sons Inc, ISBN 0-471-35457-0, 1086 p. 2001.

3. Merritt, Herbert E. Hydraulic Control Systems. John Wiley & Sons, ISBN 0471596175. 357 p. 1967.

4. Jelali, Mohieddine & Kroll, Andreas. Hydraulic Servo-systems: Modelling, Identification, and Control. Springer, ISBN 1852336927, 9781852336929. 355 p. 2003.

5. Merrill, E.F. Dynamics of AC electrical machines. Industry Applications, IEEE Transactions on, Vol. 30:2. pp. 277-285. 1994.

6. Ehrich, Fredric F. Handbook of Rotordynamics. McGraw-Hill, ISBN 0070193304. 496 p. 1992.

7. Blevins, R.D. Formulas for natural frequency and mode shape, New York: Van Nostrand Reinhold, ISBN 0-442-20710-7. 492 p. 1979.

8. Junger, M. C. & Feit, D. Sound, Structures, and Their Interaction. 2nd Edition. The MIT Press, Cambridge, Massachusetts, London. MA ISBN 0-262-10034-7. 448 p. 1986.

9. Everstine, G.C. Finite element formulations of structural acoustics problems. Computers & Structures, Vol. 65 (3). pp. 307-321. 1997.

10. Pani, P.K. & Bhattacharyya, S.K. Fluid-structure interaction effects on dynamic pressure of a rectangular lock-gate. Finite Elements in Analysis and Design Vol. 43. pp. 739-748. 2007.

11. Hakala, Matti. Numerical modelling of fluid-structure and structure-structure interaction. Espoo, VTT Publications / Technical Research Centre of Finland; 22. ISBN 951-38-2305-9. 62 p. 1985

12. Klinge, P., Äärettömät elementit. (in finnish) Master's Thesis. Helsinki University of Technology. Espoo. 124 p. 1985.

13. Everstine, G.C. A symmetric potential formulation for fluid-structure interaction. Journal of Sound and Vibration, Vol. 79:1. pp. 157-160. 1981.

14. Abaqus Theory Manual, version 6.8.2 Dassault Systèmes Simulia Corp., Providence, RI, USA. 2008.

15. Amabili, M., Dalpiaz, G. & Santolini, C. Free vibration of free-edge circular plates immersed in water. Proceedings of the 12th International Modal Analysis Conference, Honolulu, HI, pp. 349-355. 1994.

16. Kwak, M.K. Vibration of Circular Plates in Contact with Water, Journal of Applied Mechanics, Vol. 58. pp. 480-483. 1991.

17. Amabili, M. & Kwak, M.K. Free Vibrations of Circular Plates Coupled with Liquids: Revising the Lamb Problem. Journal of Fluids and Structures Vol. 10. pp. 743-761. 1996.

18. Patton, K. T. Tables of Hydrodynamic Mass Factors for Translational Motion. ASME Paper No. 65-WA/Unt-2, 1965.

19. LMS Cada-X Manuals Rev 3.5.F. Leuven, Belgium: LMS International. n.d.

20. LMS TestLab Manuals Rev 8B. Leuven, Belgium: LMS International. 2007.

21. Peeters, B et al. The PolyMAX frequency-domain method: a new standard for modal parameter estimation?. Shock and Vibration, Vol. 11 pp. 395-409. 2004.

22. Ewins, D. J. Modal Testing: Theory, Practice and Application. Second edition. England: Reseach Studies Press Ltd. ISBN 0-86380-218-4. 562 p. 2000.

23. Heylen, W. & Lammens, Stefan, & Sas. Paul. Modal Analysis Theory and Testing. Belgium: Katholieke Universiteit Leuven. ISBN 90-73802-61-X. 1997.

24. Peeters, B. & Auweraer, HV. Polymax: A Revolution in Operational Modal Analysis. 1st International Operational Modal Analysis Conference. 2005.